

Dynamics of conduction blocks in a model of paced cardiac tissue

Hervé Henry* and Wouter-Jan Rappel

Center for Theoretical Biological Physics University of California San Diego 9500 Gilman Drive, La Jolla, California 92093, USA

(Received 22 April 2004; revised manuscript received 15 November 2004; published 31 May 2005)

We study numerically the dynamics of conduction blocks using a detailed electrophysiological model. We find that this dynamics depends critically on the size of the paced region. Small pacing regions lead to stationary conduction blocks while larger pacing regions can lead to conduction blocks that travel periodically towards the pacing region. We show that this size-dependence dynamics can lead to a novel arrhythmogenic mechanism. Furthermore, we show that the essential phenomena can be captured in a much simpler coupled-map model.

DOI: 10.1103/PhysRevE.71.051911

PACS number(s): 87.19.Hh, 87.10.+e

I. INTRODUCTION

The coupling of the electrical excitation to the contractile forces in the heart is essential to the blood supply to the body. Abnormal electrical activity, in particular arrhythmias, can have dire consequences. The most serious of all, ventricular fibrillation (VF), is characterized by disordered electrical activity within the ventricles and leads to death within minutes.

Unfortunately, the precise cause of the onset and maintenance of VF remains elusive. It is believed, however, that electrical wave reentry plays an important role. Reentry is initiated when an electrical wave is locally blocked, leading to a broken wave front that can reexcite the tissue behind the conduction block. There are several ways to create a conduction block. Perhaps the most intuitive one is an anatomical tissue heterogeneity through which the electrical wave fails to propagate [1,2]. Although these heterogeneities exist and play a role in the initiation of VF, recently a new mechanism for conduction block in perfectly *homogeneous* tissue has been described in models [3–5] and experiments [6,7]. A key contributor to this *dynamical* heterogeneity is electrical alternans, which is characterized by a beat to beat oscillation in the action potential duration (APD, defined below) under rapid pacing conditions. Clinically, the occurrence of T wave alternans in ECGs has been associated with sudden cardiac arrest [8,9]. In isolated cells, the onset of alternans can be determined from the restitution curve which relates the APD to the diastolic interval (DI), the time interval between two successive action potential. If this curve has a slope larger than 1, it is easy to see that a period doubling bifurcation develops, resulting in an APD that is alternately short and long [10,11]. This simple vision, however, is most likely not complete as memory effects [12] and calcium cycling effects [13,14] have been shown to play a role in the mechanism leading to alternans.

In the case of spatially extended systems, the possible dynamical behavior becomes more complicated. The conduction velocity also depends on the DI, which can lead to a

spatial modulation of the alternans, called discordant alternans [3,4]. During discordant alternans, the APD is following a long-short-long pattern in one region of the cable and a short-long-short pattern in another. Separating these regions are nodes where the APD is constant. They can be either stationary or traveling. In addition, during discordant alternans, the amplitude of the alternans (the difference between APDs in subsequent beats) can grow when moving away from the pacing site. Hence, at a critical distance, provided the amplitude of alternans is large enough, the tissue can no longer support a traveling wave for each excitation and a diffusive conduction block [15] develops: a wave will propagate over a given distance along the cable and will then come to a stop.

Here, we study the dynamics of the conduction blocks using a detailed electrophysiological model and a pacing domain of variable size. We present a quantitative and qualitative description of the observed patterns and present results from numerical experiments in cables and sheets of cardiac tissue. Our main results are (i) in addition to a stationary conduction block, rapid pacing can lead to periodic patterns of moving conduction blocks, (ii) the type of conduction block is critically dependent on the size of the pacing region, and (iii) these effects combined can lead to a novel mechanism for reentry. Furthermore, we show that a simple coupled-map model gives qualitatively similar results.

II. MODELING OF A CABLE OF CARDIAC CELLS AND TERMINOLOGY

To describe the electrophysiological properties of cardiac tissue, we used the reaction-diffusion equation,

$$\partial_t V = D \nabla^2 V - (\sum_{ion} I_{ion} + I_{stim}) / C, \quad (1)$$

where V is the transmembrane potential, $C = 1 \mu\text{F cm}^{-2}$ is the membrane capacitance, $D \nabla^2$ with $D = 0.001 \text{ cm}^2 \text{ s}^{-1}$, expresses the intercellular coupling, I_{ion} represents the different transmembrane currents, and I_{stim} is the applied pacing current. The ionic currents in I_{ion} are governed by nonlinear evolution equations coupled to V , and here we have chosen to use a modified version of the Luo-Rudy model [16] to describe these currents. A detailed description of this model and our modifications are given in Appendix A. The integra-

*Present address: Laboratoire de Physique de la Matière Condensée, Ecole Polytechnique, 91128 Palaiseau, France.

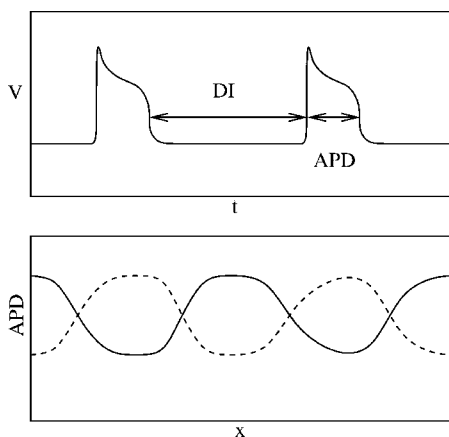


FIG. 1. Top: Schematic time course of the transmembrane potential at a point during normal cardiac rhythm (i.e., without alternans). The diastolic interval (DI) is the period of time during which the transmembrane potential is below a given value and the action potential duration (APD) is the period of time during which the action potential is over this threshold value. Bottom: Schematic drawing of the APD along the cable during an even beat (solid line) and an odd beat (dashed line) in the discordant alternans regime. In the case of normal cardiac rhythm (i.e., without alternans), both lines would be the same and the APD would be constant in space [except at the pacing site (the end of the cable) where boundary effects tend to lengthen (shorten) the APD]. In the case of concordant alternans, the APD during successive beats would be different but constant along the cable (apart from boundary effects).

tion scheme we used was forward Euler with space and time discretizations of $\delta x = 0.025$ cm and $\delta t = 0.02$ ms, respectively. Finally, the space constant was determined to be 0.06 cm.

The cable was paced at one end with a period T through a 1-ms-long constant current stimulus of $I_{stim} = -80 \mu\text{A}/\text{cm}^2$ [26]. The pacing domain consisted of n grid points, where n was varied between 1 and 20, thus corresponding to a pacing domain ranging in size from 0.025 cm to 0.5 cm [27]. As we will see below, changing the number of stimulated grid points can have a dramatic effect. On the other hand, changing the size of the simulation cable from 10 cm, the length used here, to 5 cm did not reveal any qualitative differences. This, along with the fact that the propagation speed from endocardium to epicardium can be much smaller (about 17 cm/s) [17] than the one used here (about 51 cm/s), implies that the observations reported here might be relevant to human ventricles. Finally, additional simulations performed using either a stronger stimulus or a longer stimulus showed little effect.

We define the beginning of an action potential at position x as the moment when $V(x, t)$ crosses a threshold value V_{th} from below. Similarly, the end of the action potential is defined as the moment when $V(x, t)$ decreases below V_{th} . The APD is then defined as the time difference between these two events (see Fig. 1). Then, the DI is defined as the time between the end of one action potential and the beginning of the next (see Fig. 1). A conduction block for the m th stimulus occurs at the i th grid point when an action potential was elicited at the i th-1 grid point by the m th stimulus but not at

the i th one. V_{th} was chosen to be equal to -60 mV and changes in the value of V_{th} (between -80 mV and -50 mV) did not affect results significantly. In addition, it is useful to define a waveback and a wavefront. A wavefront is the boundary between a region at rest and an excited region when the latter region is invading the former, while the waveback is the boundary when the former is invading the latter.

The pacing periods used here (≈ 160 ms) are short compared to the normal pacing period in humans. Of course, this pacing period is dictated by the choice of the electrophysiological model used here.

III. RESULTS IN A CABLE

Let us first consider a one-dimensional cable. For a small enough pacing period, a period doubling instability to alternans takes place. After a transient regime where the amplitude of alternans grows, a steady state is reached. This regime is characterized by the fact that each stimulus will elicit an action potential all along the cable and that the action potentials elicited by two successive stimuli at a given point in space will have different durations (a short action potential follows a long one which follows a short one, and so on) [18]. This allows us to define, at a given point in space x , the amplitude of alternans, $a(x, m)$, for the m th stimulus as the difference between the APD due to this stimulus and the APD due to the previous stimulus multiplied by $(-1)^m$ so that a does not change sign every stimulus. In the case of concordant alternans, a is roughly constant in space and does not change sign. In our simulations, however, since the size of the simulated cable is bigger than the characteristic wavelength of alternans [19], we observe discordant alternans. In this case, $a(x, m)$ is not constant in space and changes sign when going along the cable. For example, if a point in the cable with positive a exhibits a sequence of beats that is long short-long-short... then a point of the cable with negative a will exhibit a sequence of beats that is short-long-short-long... . Consequently, between regions of opposite a , there is a point where $a=0$, corresponding to an alternans node.

In the case of discordant alternans, one can observe two distinct regimes (see [19] for a full theoretical analysis) that are characterized by the spatio-temporal evolution of a . The first regime, called standing alternans, is characterized by stationary alternans nodes. This is shown in Fig. 2(a1), where we show a gray-scale space-time plot of a . In contrast, the alternans nodes in the second regime, called traveling-wave alternans, are nonstationary and are traveling towards the pacing site. This is illustrated in Fig. 2(a2), which shows that a is changing slowly in time with a given period. In addition, in this regime, $a=0$ at the pacing site and $|a|$ increases when moving away from the pacing site.

A change in the dynamics of the alternans nodes was observed earlier in the theoretical study of Echebarria and Karma [19]. There, this change was accomplished by changing the properties of the tissue (i.e., by changing the model). Here, in contrast, the only difference between the simulations shown in Figs. 2(a1) and 2(a2) is the size of the pacing region: $n=6$ in (a1) and $n=10$ in (a2). This finding already

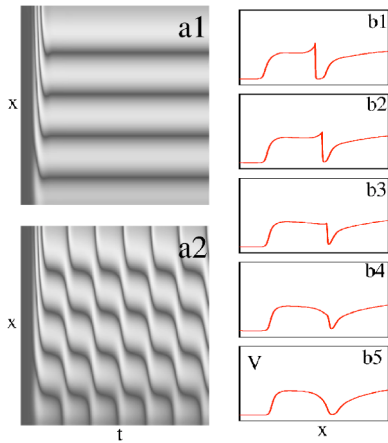


FIG. 2. (a1) and (a2) Gray-scale time-space plot of the alternans amplitude $|a(x,m)|$ with black corresponding to $a(x,m)=0$ and white corresponding to large values of the amplitude. The pacing period in both figures is 162 ms and the number of pacing grid points is $n=6$ in (a1) and $n=10$ in (a2). In (a1), one can see discordant alternans where the nodes, regions of zero amplitude (and thus in black), are not moving. In (a2), the discordant alternans leads to nodes that are traveling towards the pacing site. (b1)–(b5): Successive profiles of $V(x)$, taken at 20 ms intervals, during a conduction block event. The waves are initiated on the left-hand side of the cable. In (b1), one can see an action potential propagating from the left towards the right with its typical sharp wavefront. The smoother waveback of the wave due to the previous stimulus is on the right-hand side of the plot. The wavefront propagates faster than the wave back [(b1)–(b3)] and finally reaches a region that has not yet recovered and cannot be rapidly activated. Reaching this region (b4), the wave comes to a stop and fails to propagate further (this is called throughout this paper a conduction block). In (b5), one can see that the sharp wavefront has disappeared. The cable is 10 cm long and V ranges from -100 mV to 100 mV.

shows that the size of the pacing region may play a critical role in the alternans-induced arrhythmias. A rationale for the effect of changing the size of the pacing region will be given later in the manuscript (end of Sec. V).

Decreasing the stimulation period further leads to conduction blocks. In other words, some stimuli are not able to create an action potential that propagates all along the cable. Two different types of conduction blocks were observed: (i) *conduction block at the pacing site*; the stimulus is not able to elicit an action potential at all and (ii) *conduction block away from the pacing site*; the stimulus creates an action potential that begins to propagate along the cable and this action potential fails to propagate at a given point in space away from the pacing site. The latter type of conduction block is illustrated in Figs. 2(b1)–2(b5). Hence, a conduction block can be characterized by the point in space where it took place and also by the index of the stimulus that created the action potential which failed to propagate at this point.

In our simulations, we found that the dynamics of the conduction blocks depends on both the size of the paced region and on the pacing period. Examples of the observed dynamics of the conduction blocks are illustrated in Fig. 3, where we plot the position of the conduction block as a function of the pacing cycle number m . In Figs. 3(a) and

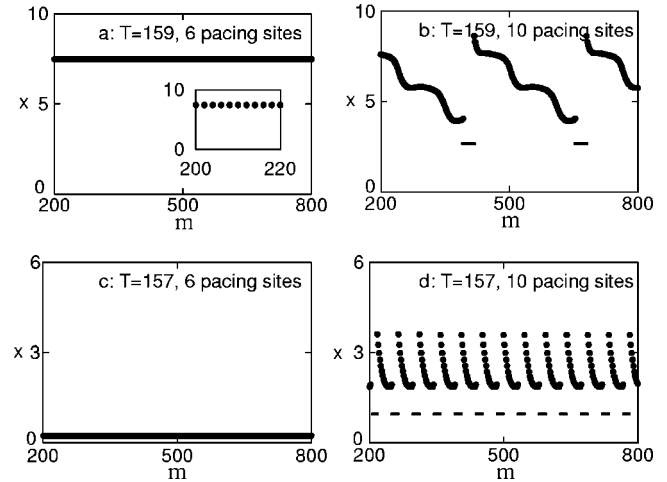


FIG. 3. Position of the conduction block as a function of the stimulus number m for different pacing period T (in ms) and pacing region sizes n . In (a), the inset shows that the conduction block leads to a 2:1 rhythm. In both (b) and (d), the conduction block travels towards the pacing site during a number of stimuli, followed by a small number of stimuli during which there is no conduction block. In (b) and (d), the thick lines correspond to the stimuli where no conduction block is observed. One should note the similarity between the trajectories of conduction blocks for $T=159$ ms and $n=10$ ($n=6$) and the trajectories of the alternans nodes for $T=162$ ms and $n=10$ ($n=6$) shown in Figs. 2(a1) and 2(a2).

3(c), the block occurs at a fixed location (either away from the pacing site or at the pacing site) once every other stimulus (i.e., a 2:1 rhythm). Examples of more complex behavior are illustrated in Figs. 3(b) and 3(d) where the location of the conduction block is nonstationary and forms a periodic pattern. In these cases, a conduction block forms at a certain location away from the pacing site. In subsequent beats, the position of this conduction block moves closer to the pacing site (during this regime every other stimulus is blocked). Eventually, the block disappears, after which no conduction blocks are observed during several pacing cycles (i.e., propagation with a discordant alternans pattern). Then, the conduction block reforms at precisely the same location as previously and the sequence restarts.

This gives rise to a periodic pattern of conduction blocks with a certain “amplitude,” defined here as the distance between the site where the conduction block first forms and the site where the conduction block disappears. We found that this amplitude can take on values between 2 cm [see Fig. 3(d)] and 5 cm [see Fig. 3(b)] and that for a given pacing period, both the amplitude of the conduction block wave and its period were dependent on the number of pacing grid points. We also found that the trajectory of the conduction blocks in Fig. 3(b), which is close to the onset of conduction blocks, is strikingly similar to the dynamic pattern of the location of the alternans nodes shown in Fig. 2(a2). These alternans nodes also display periodic movement towards the pacing site with slow movement followed by fast movement. This movement is presumably due to the use of zero flux boundary conditions, which favors the existence of an extremum at the boundaries: slow movement corresponds to an

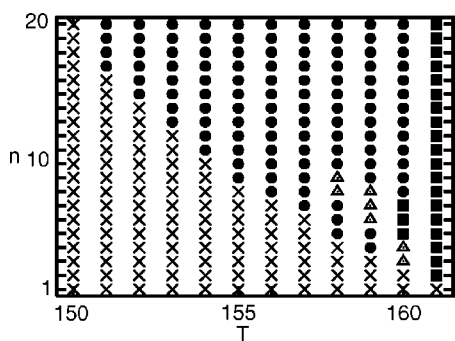


FIG. 4. Phase diagram showing the type of conduction block: filled circles represent periodic conduction block waves, crosses represent stationary conduction blocks at the pacing site, triangles represent stationary conduction blocks away from the pacing site, and filled boxes represent no conduction block (i.e., discordant or concordant alternans.). T is expressed in ms.

extremum of the alternans amplitude near the boundary while fast movement corresponds to an alternans node near the boundary. A phase diagram representing the nature of conduction blocks as a function of the number of pacing grid points and of the period is shown in Fig. 4. It is also worth mentioning that the use of slightly irregular pacing times, modeled via the inclusion of a noise term with a variance of 1 ms, did not change significantly the phase diagram.

IV. RESULTS IN A SHEET OF CARDIAC TISSUE

From the above, it should now be clear how a slight inhomogeneity in the size of the pacing area can lead to reentry. Envision a 2D sheet of cardiac tissue [modeled by Eq. (1) using two space variables instead of one], paced from one side by a domain containing two widths, n for the upper part and n^* for the lower part, as shown in Fig. 5. Neglecting spatial coupling in the direction perpendicular of the wave propagation, the lower and upper part of the tissue will see waves originating from domains with different sizes. Reentry should be possible when the spatial locations of the conduction blocks in the two domains are significantly different. Then, the electrical wave will be blocked in one part of the tissue while propagating normally in the other part, leading to the excitation of the tissue behind the conduction block and to reentry.

We can estimate the likelihood of reentry in 2D, paced by domains of size n and n^* , based on our 1D results. Reentry is likely when (i) a cable paced with n shows a conduction block while a cable paced with n^* does not exhibit a conduction block, or vice versa, or (ii) the difference in spatial location between the conduction blocks in cables paced with n and n^* becomes large. We found that for $n^* = n \pm 1$, one or both of these conditions were met in most of the phase space for which conduction blocks occur away from the pacing site (i.e., filled circles in Fig. 4). In most cases, the conditions were met within a few hundred stimuli while occasionally a larger number of stimuli was necessary.

Of course, the preceding arguments neglect spatial coupling perpendicular to the wave-propagation direction. Nev-

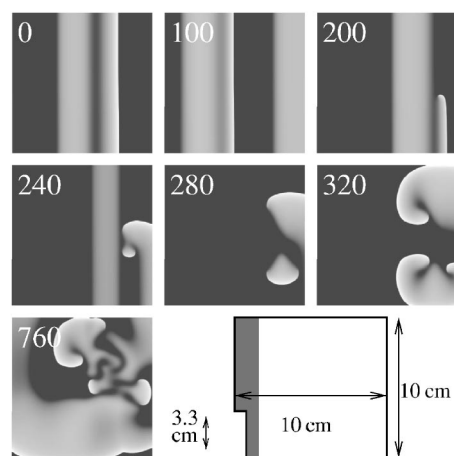


FIG. 5. Series of gray-scale plots showing the birth of a spiral wave. Time (shown in ms) is arbitrarily set to 0 at the start of the last stimulus. The gray scale represents the membrane potential values with white corresponding to maximum depolarization and black corresponding to maximum repolarization. At $t=0$ ms, one can see the wave elicited by the previous stimulus propagating from left to right. Because of the discordant alternans, the APD differs strongly across the sheet with the leftmost clear stripe corresponding to a region where the APD is long (it is not a propagating wave despite the cells in this region being depolarized [15]) and the central dark stripe corresponding to a region where the APD is short. At $t=100$ ms, one can see on the left-hand side of the plot the wave elicited by the next stimulus, while on the right-hand side one can see the waveback of the wave seen in the $t=0$ ms frame. At $t=200$ ms, a conduction block occurred in the top part of the sheet while in the bottom part the wave was able to continue to propagate. This partial wave block results in a broken wave front which leads to the birth of reentry, as can be seen in the $t=240$ ms, 280 ms, and 320 ms frames. As this wave front curls and attempts to reenter previously excited tissue with a long repolarization time (gray stripe in $t=240$ ms frame), it breaks up into two spiral tips ($t=280$ ms). Finally at $t=760$ ms, one can see that further instabilities have led to a disordered activity similar to ventricular fibrillation. The geometry of the computational domain is also shown schematically, where the gray region, exaggerated for clarity, corresponds to the cells that are paced. The width of the bottom part of this region is $n^*=8$ and that of the top part is $n=9$ grid points.

ertheless, we found that the phase diagram was a valuable predictor for the occurrence of reentry in full-scale 2D simulations. A typical example of our 2D simulations, performed using the same numerical scheme as in our one-dimensional simulations, is displayed in Fig. 5, where we show a series of gray-scale plots of the membrane potential, with black corresponding to repolarized tissue and white corresponding to depolarized tissue. In this example, the width of the two pacing domains differed by a single grid point: $n^*=8$ versus $n=9$. Both domains are paced with a constant period of 158 ms, leading to traveling conduction blocks with slightly different periodicity. During the roughly 100 first stimuli, the position of the conduction block was nearly identical in the upper and lower parts of the tissue. During the subsequent stimulus, however, a wave block remains in the upper part of the tissue but *not* in the lower part of the tissue, which now allows unblocked propagation [see Figs. 3(b) and 3(d)]. As

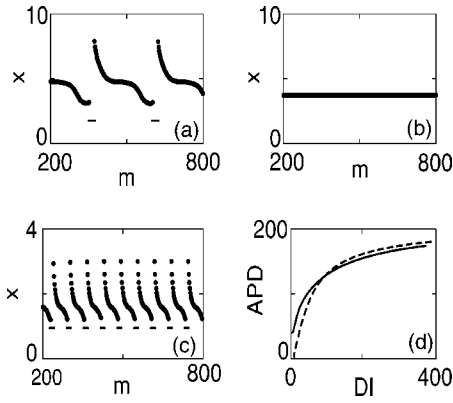


FIG. 6. (a)–(c) Position of the conduction block as a function of the stimulus for different pacing period and pacing region sizes calculated using the coupled-map model [(a) $T=161$ ms, $n=20$; (b) $T=161$ ms, $n=10$; (c) $T=156$ ms, $n=12$]. In (a) and (c), the thick lines correspond to the stimuli where no conduction block is observed. (d) The restitution curve used in the model for the single element (solid line) and for the cable (dashed line). Note that the slope of the single cell curve is smaller than the slope of the whole cable curve.

time progresses, the propagating wave in the lower part reenters the upper part behind the wave block, leading to a spiral wave. For clarity, we have stopped stimulating the tissue once the reentry appeared, although we have verified that continuous stimulation also resulted in long-lasting reentry. In addition, we have checked that smaller domains were also able to produce reentry and that using a line of stimulation with a thickness varying randomly can also lead to sustained reentry.

V. COUPLED MAP MODEL

The results from the full ionic model can be reproduced by a coupled map model similar to the ones used in previous work [7,19]. To describe the dynamics of alternans nodes and conduction blocks, we consider the following two fields: $T_{up}(x,n)$, which is the time at which an action potential is elicited in x due to the n th stimulus, and $T_{rep}(x,n)$, which is the time at which it ends. The equation for the repolarization time T_{rep} is the same for both the cable and the pacing domain,

$$T_{rep}(x,n) = T_{up}(x,n) + \text{APD}[\text{DI}(x,n)] + \xi^2 \nabla^2 T_{rep}(x,n) + w \partial_x T_{rep}(x,n). \quad (2)$$

The first two terms in this equation express the fact that a single cell repolarizes at time T_{up} plus the duration of the action potential. The latter is taken from the restitution curve $\text{APD}(\text{DI})$. For the paced domain, this curve is calculated using a single cell while for the cable it is calculated 1 cm away from the pacing domain, taken to be large. In this region of the cable, we found that the restitution curve was minimally affected by the proximity of the pacing domain and that the dispersion of repolarization due to alternans was minimal. The two restitution curves are shown in Fig. 6(d). The last two terms take into account spatial effects: the dif-

fusion term indicates the perturbation due to intercellular coupling (we consider here that the repolarization wave is a phase wave and does not correspond to the propagation of a wave back) and the last term expresses the asymmetry introduced by the pacing at one end of the cable [19]. The length scales ξ and w were chosen here to reproduce the phase diagram of Fig. 4 in a semiquantitative fashion.

The equation describing T_{up} in the pacing domain is $T_{up}(x,n) = T_n$, with T_n being the pacing period, while in the cable it is given by

$$T_{up}(x,n) = T_n + \int_0^x dx' \frac{1}{c[\text{DI}(x',n)]}, \quad (3)$$

where c is the propagation speed of the wave front. This propagation speed is a function of the DI, which itself is of course a function of x and is the difference between the arrival of the n th action potential at x and the repolarization following the $(n-1)$ th stimulus: $\text{DI}(x,n) = T_{up}(x,n) - T_{rep}(x,n-1)$.

The restitution curve also determined the occurrence of a conduction block: we defined a conduction block to take place when the restitution curve had no value for the diastolic interval computed from Eq. (3). In this case, we computed the repolarization times between the origin and the position of the conduction block using Eq. (2) along with boundary condition $T_{rep} = T_{up}$ at the site of the conduction block. The repolarization time for the remainder of the cable (i.e., behind the conduction block) was set to the repolarization time computed at the previous stimulus, except in a small transition region, in size equal to ξ , immediately behind the conduction block. There, a simple sigmoidal function was used that smoothly connected the repolarization times on both sides of this region.

The reduced model is able to capture the essential features of the full ionic model, including the striking dependence on the size of the pacing region for both the alternans nodes and the conduction blocks dynamics. The latter is shown in Figs. 6(a)–6(c), where we plot the position of the conduction block as a function of pacing cycle for $w=0.025$ and $\xi^2=0.04$, which are comparable to the values presented in Table I of Ref. [19] when considering a full ionic model. All qualitative features of Fig. 3 can be readily recognized, including traveling conduction blocks with a large amplitude (a) [28], traveling conduction blocks with a small amplitude (c), and stationary conduction block away from the pacing domain (b). Not shown here, but also found within the reduced model, is a 2:1 conduction block at the pacing site. For the values of w and ξ employed here, the boundaries between the different types of conduction block in the phase diagram derived from the full model and the coupled-map model differed by at most 5 ms.

Both the full ionic model and coupled map model show, for certain pacing periods, a transition from stationary conduction blocks to traveling conduction blocks as the size of the pacing domain is increased. Interestingly, a similar transition also occurs in the dynamics of alternans nodes when one increases this size. To understand the effect of changing

the size of the pacing region on the nature of alternans, we consider the equation for the amplitude a of the alternans derived in [19],

$$\partial_x a = \sigma a - \int_0^x dx' \frac{a}{\Lambda} - \tilde{w} \partial_x a + \tilde{\xi}^2 \partial_{xx} a - g a^3. \quad (4)$$

Here, σa represents a linear growth term, $g a^3$ is a nonlinear restabilizing term, and Λ , \tilde{w} , and $\tilde{\xi}$ are length scales which are *a priori* different from the ones w and ξ used in Eqs. (2) and (3). The transition between traveling nodes in our simulations (large pacing domains) and standing nodes (smaller pacing domains) can be understood when realizing the size of the pacing domain dictates the boundary condition at $x=0$ of Eq. (4). Pacing a cable using a large piece of tissue results in a pacing domain that essentially behaves as a single isolated cell. If the restitution curve of a single cell [solid line in Fig. 6(b)] has a slope less than 1, this domain will not display alternans and the amplitude equation needs to be solved with boundary condition $a=0$. For a smaller pacing domain, however, spatial coupling becomes important and the relevant restitution curve becomes steeper [dashed line in Fig. 6(b)], which can lead to alternans. Thus, for smaller domains the relevant boundary condition for the amplitude equation is $\partial_x a=0$. A standing-wave solution to the amplitude equation can be described by $a=a_0 \cos(2\pi\lambda x + \phi)$, where $1/\lambda$ is the separation between the nodes. This solution (with $a_0 \neq 0$) can only satisfy the $\partial_x a=0$ boundary condition and *not* the $a=0$ boundary condition. This is easy to see when one considers the standing-wave solution in Eq. (4) at $x=0$: the only nonzero term on the r.h.s. is $\partial_x a$ which requires $a_0 2\pi/\lambda=0$ and finally $a_0=0$. Hence, a standing-wave solution is only possible for small pacing sizes, and increasing the size of the pacing domain suppresses the standing-wave solution. It is likely that this qualitative change in the nature of allowed solutions underlies the transition between stationary to traveling blocks observed in the ionic and coupled map model.

VI. DISCUSSION

To conclude, we have found that the spatio-temporal structure of alternans and the dynamics of conduction blocks is strongly influenced by both the size of the paced domain and the pacing period. This dependence provides a novel arrhythmogenic mechanism which we illustrate in a homogeneous two-dimensional sheet of tissue, paced by two domains that vary slightly in size. The reentry is initiated through pacing with a constant period and hence does not require an abruptly changing pacing frequency nor a symmetry-breaking change of location as in previous studies [3]. We have found, using different ionic models, including a detailed canine model [7] and the simplified three-variable Fenton-Karma model [20,21], that the results we present here are partially model-dependent. This is perhaps not surprising, as other arrhythmogenic mechanisms have been shown to depend on the details of the electrophysiological model [22]. Nevertheless, a reduced coupled map model was able to reproduce, both qualitatively and, to some degree,

quantitatively, the results presented here. Consequently, we expect that the dynamics of conduction blocks will depend critically on the pacing protocol in a wide range of detailed models.

Of course, the ultimate test should come in the form of experimental studies similar to the one conducted by Fox *et al.* [7] but with a varying in size stimulation region. It should be possible to conduct quantitative studies of Purkinje fibers, which conduct the electrical stimulus in an actual heart to the ventricles and which penetrate the heart wall to varying depths. These fibers can be isolated, resulting in linear strands of cardiac tissue [7]. On the theoretical side, a further extension of this work will be the formulation of a coupled map model which takes into account the effects of coupling transversely to the propagation direction of the wave.

ACKNOWLEDGMENTS

The authors would like to thank Flavio Fenton and Jeffrey Fox for useful discussions. They also would like to thank Alain Karma for a critical reading of this manuscript. Computations were performed in part on the National Science Foundation Terascale Computing System at the Pittsburgh Supercomputing Center. We acknowledge the National Biomedical Computation Resource (NIH P41 RR-08605). This research was supported in part by the NSF-sponsored Center for Theoretical Biological Physics (Grants No. PHY-0216576 and No. 0225630) (H.H. and W.J.R.), and by NIH Grant No. HL075515-01 (W.J.R.).

APPENDIX A: DESCRIPTION OF THE MODEL

The Luo-Rudy model [16], and its subsequent refinements (see, e.g., [23]), have been widely used either in their original form or in modified forms in numerical studies of wave propagation in cardiac tissue [24]. The model describes the voltage and time dependence of the ionic currents $\sum_{ion} I_{ion}$ used in the equation for the transmembrane potential V of a single cell,

$$C \frac{dV}{dt} = - \sum_{ion} I_{ion}, \quad (A1)$$

where C is the membrane capacitance. In the original Luo-Rudy model, the total ionic current is given as

$$\sum_{ion} I_{ion} = - (I_{Na} + I_{si} + I_K + I_{K1} + I_{Kp} + I_b), \quad (A2)$$

where $I_{Na} = G_{Na} m^3 h j (V - E_{Na})$ is the fast sodium current, $I_{si} = G_{si} d f (V - E_{si})$ is the slow inward current representing the L-type calcium current, $I_K = G_{Kxx1} (V - E_K)$ is the time-dependent potassium current, $I_{K1} = G_{K1} K1_\infty (V - E_{K1})$ is the time-independent potassium current, $I_{Kp} = G_{Kp} K_p (V - E_{Kp})$ is the plateau potassium current, and $I_b = G_b (V - E_b)$ is the background current. In these expressions, m , h , j , d , f , and x are gating variables describing the opening and closing of ionic channels and the dynamics of these variables is described by nonlinear ordinary differential equations of the form

$$\frac{dy}{dt} = \frac{y_{\infty}(V) - y}{\tau_y(V)}, \quad (\text{A3})$$

where y represents one of the gating variables. Finally, the equations for the currents are supplemented by an expression for the calcium concentration,

$$\frac{[\text{Ca}]_i}{dt} = -10^4 I_{si} + 0.07(10^{-4}[\text{Ca}]_i). \quad (\text{A4})$$

Explicit expressions for the constants can be found in the original work of Luo and Rudy (Ref. [16]). Here, we have made two modifications to allow propagation of spiral waves in a small system. First, we have reduced G_{si} from 0.09 to 0.055. Second, we have sped up the calcium dynamics by altering the time scales of the d and f gates. Specifically, both τ_d and τ_f were multiplied by 0.8.

Initial conditions that were used consisted of a cable initially polarized that was then paced with decreasing intervals between stimuli until the desired period was reached.

-
- [1] F. Akar, G. Yan, C. Antzelevitch, and D. Rosenbaum, *Circulation* **105**, 1247 (2002).
- [2] H. Henry and W.-J. Rappel, *Chaos* **14**, 172 (2004).
- [3] Z. Qu, A. Garfinkel, P. S. Chen, and J. N. Weiss, *Circulation* **102**, 1664 (2000).
- [4] M. A. Watanabe, F. H. Fenton, S. J. Evans, H. M. Hastings, and A. Karma, *J. Cardiovasc. Electrophysiol.* **12**, 196 (2001).
- [5] J. J. Fox, R. Gilmour, and E. Bodenschatz, *Phys. Rev. Lett.* **89**, 198101 (2002).
- [6] J. M. Pastore, S. D. Girouard, K. R. Laurita, F. G. Akar, and D. S. Rosenbaum, *Circulation* **99**, 1385 (1999).
- [7] J. J. Fox, M. L. Riccio, F. Hua, E. Bodenschatz, and R. F. Gilmour, *Circ. Res.* **90**, 289 (2002).
- [8] D. S. Rosenbaum, L. E. Jackson, J. M. Smith, H. Garan, J. N. Ruskin, and R. J. Cohen, *N. Engl. J. Med.* **330**, 235 (1994).
- [9] N. A. Estes 3rd, G. Michaud, D. P. Zipes, N. El-Sherif, F. J. Venditti, D. S. Rosenbaum, P. Albrecht, P. J. Wang, and R. J. Cohen, *Am. J. Cardiol.* **80**, 1314 (1997).
- [10] J. B. Nolasco and R. W. Dahlen, *J. Appl. Physiol.* **25**, 191 (1968).
- [11] M. Guevara, F. Alonso, D. JeanDubeux, and A. van Ginneken, in *Cell to Cell Signalling: From Experiments to Theoretical Models*, edited by A. Goldbeter (Academic, London, 1989), pp. 551–563.
- [12] J. J. Fox, E. Bodenschatz, and R. F. Gilmour, *Phys. Rev. Lett.* **89**, 138101 (2002).
- [13] Y. Shiferaw, M. A. Watanabe, A. Garfinkel, J. N. Weiss, and A. Karma, *Biophys. J.* **85**, 3666 (2003).
- [14] E. J. Pruvot, R. P. Ktra, D. S. Rosenbaum, and K. R. Laurita, *Circ. Res.* **94**, 1083 (2004).
- [15] V. N. Biktashev, *Phys. Rev. Lett.* **89**, 168102 (2002).
- [16] C. H. Luo and Y. Rudy, *Circ. Res.* **68**, 1501 (1991).
- [17] M. Pressler, P. Münster, and X. Huang, *Cardiac Electrophysiology, From Cell to Beside*, 2nd ed., edited by D. P. Zipes and J. Jalife (Saunders Company, 1995), Chap. 16, pp. 144–151.
- [18] T. J. Lewis and M. R. Guevara, *J. Theor. Biol.* **146**, 407 (1990).
- [19] B. Echebarria and A. Karma, *Phys. Rev. Lett.* **88**, 208101 (2002).
- [20] F. H. Fenton, E. M. Cherry, H. M. Hastings, and S. J. Evans, *Chaos* **12**, 852 (2002).
- [21] F. Fenton and A. Karma, *Chaos* **8**, 20 (1998).
- [22] W.-J. Rappel, *Chaos* **11**, 71 (2001).
- [23] C. H. Luo and Y. Rudy, *Circ. Res.* **74**, 1071 (1994).
- [24] Z. Qu, F. Xie, A. Garfinkel, and J. N. Weiss, *Ann. Biomed. Eng.* **28**, 755 (2000).
- [25] A. Yehia, D. Jeandubeux, F. Alonso, and M. Guevara, *Chaos* **9**, 916 (1999).
- [26] The threshold stimulus is approximately $-30 \mu\text{A}/\text{cm}^2$ when pacing 10 cells of the cable or when pacing a single cell and goes up to approximately $-45 \mu\text{A}/\text{cm}^2$ when pacing a single cell of the cable.
- [27] In order to check that our results are not due to a change in the total stimulation current, we performed additional simulations. In these simulations, we kept the total stimulation current (nI_{stim}) constant by choosing $I_{stim} = -800/n \mu\text{A}/\text{cm}^2$. This change in stimulation protocol did not significantly alter our results; the dynamics of conduction blocks away from the pacing site was unchanged while conduction blocks at the pacing site occurred for slightly smaller values of n or slightly smaller pacing period T . Hence, the results we report here cannot be attributed to a change in total stimulation amplitude as in [25].
- [28] In this case, one should note that while in Fig. 3 three plateaus of slowly moving conduction blocks are present, in Fig. 6(a) there are only two plateaus.